



# Numerical simulations of accretion disks and astrophysical jets

P. Rossi<sup>1</sup>, G. Bodo<sup>1</sup>, A. Mignone<sup>1,2</sup>, S. Massaglia<sup>2</sup>, and A. Ferrari<sup>2</sup>

<sup>1</sup> Istituto Nazionale di Astrofisica – Osservatorio Astronomico di Torino, Via Osservatorio 20, I-10025 Pino Torinese, Italy, e-mail: rossi@oato.inaf.it

<sup>2</sup> Dipartimento di Fisica Generale, Università di Torino Via P. Giuria 1, I-10125 Torino, Italy

**Abstract.** We present the results of high resolution numerical simulations concerning accretion disks and relativistic jets. For accretion disks, in the context of the problem of angular momentum transport, we performed simulations of the magnetorotational instability in the shearing box approximation and, on the basis of our results, we discuss its validity. In the case of relativistic jets, we analyse how their interaction with the ambient medium can lead to their deceleration, as it appears to be the case for jets in FRI extragalactic radiosources.

**Key words.** Methods: numerical, MHD, accretion disks, Galaxies: jets

## 1. Introduction

The interplay between accretion and outflow is an important issue in many astrophysical contexts such as, for example, Young Stellar Objects, Active Galactic Nuclei and X-ray binaries. Accretion and outflows appear to be intimately linked phenomena, in fact, in all these environments the formation of outflows appears to be an almost unavoidable consequence of the presence of an accretion disk. The modelling of outflows can thus provide important clues on the properties of the central engine and, on the other hand, understanding the accretion process is an essential key for understanding the whole phenomenology of these objects.

Numerical simulations represent an essential tool for studying the physical processes involved in the accretion and jet contexts and

---

*Send offprint requests to:* P. Rossi

in the connection between the two, due to the complex nonlinear phenomena involved. In this note we will present two examples of numerical studies that have been performed as key-projects in the context of the INAF-CINECA agreement. The first one deals with the process of angular momentum transport in accretion disks driven by the magnetorotational instability and is presented in Section 2. The second is concerned with the problem of deceleration of relativistic jets in the context of extragalactic radiosources and is presented in Section 3. In the last section we present a summary and a discussion of future perspectives.

## 2. Angular momentum transport in accretion disks

In accretion disks, the transport of angular momentum is of particular importance since it determines the disk structure, and ultimately

the rate of accretion (see e.g. Balbus 2003). Shakura & Sunyaev (1973), by assuming that the transport of angular momentum in a disk was turbulent, were able to construct models that could reasonably reproduce the salient features of observed disk behavior. They wrote the effective turbulent viscosity in term of a parameter  $\alpha$  that incorporated all the unknown details of the turbulent process giving rise to the enhanced transport. The physical origin of the turbulence however was not discussed in their work. In fact, this aspect of their theory remained unclear for many years, until Balbus & Hawley (1991) noted that the stability of near-Keplerian disks could be changed by the presence of magnetic fields. The resulting instability, subsequently known as the Magneto-Rotational Instability (MRI), is magnetic in origin, and can lead to the growth of infinitesimal perturbations in disks that would otherwise be stable to a purely hydrodynamical evolution. It is now commonly believed that turbulence in disks is the result of the MRI growth to finite amplitude. Since the original work of Balbus & Hawley (1991), there have been numerous studies of the nonlinear evolution of the MRI directed on one hand towards understanding the process of saturation and on the other hand towards the introduction of several additional physical ingredients (Hawley & Balbus 1992; Hawley et al. 1995; Sano & Inutsuka 2001; Sano et al. 2004; Sano & Stone 2002; Turner et al. 2003). Much of the work has been performed in a local approximation called shearing box, this affords a considerable simplification over the fully cylindrical or spherical geometry. Indeed, much of what is presently known about the nonlinear evolution of the MRI is cast within its framework. Despite this big effort, several questions on the nature of MRI-driven turbulence still remain open, one of them is, in particular, the connection between local and global simulations. Ideally one should compare local and global results; however, available global disk simulations (see e.g. Hawley 2001; Hawley, Balbus & Stone 2001) have relatively low resolution while simulations with adequately high resolution are at the limit of present capabilities. Given the present re-

sources, one should at least check the self consistency of the shearing box results, by checking, for example, that the properties of the solutions do not depend on the geometrical properties of the computational domain. In our work we concentrate on the possible dependence on the box aspect ratio, i.e the size of the computational domain in the radial and azimuthal directions relative to the vertical size. Clearly a very thin box may introduce spurious effects, a very wide box rapidly becomes computationally expensive. A typical compromise is to adopt boxes with aspect ratios between the radial and vertical direction of unity. This point has not received careful consideration and there has been no systematic study of the dependence of the solutions on the aspect ratio. Furthermore, many studies in computational domains of unit aspect ratio have shown intermittent behavior associated with the formation and subsequent disruption of “channel” solutions (Hawley & Balbus 1992; Sano & Inutsuka 2001) that are the nonlinear analogues of the exponentially growing linear modes. By carrying out a study of shearing box results as a function of aspect ratio, our aim is to see whether the results observed in boxes of unit aspect ratio are representative of more extended systems, or if they display peculiarities induced by an overly constrained geometry.

We performed a series of 3D, compressible, isothermal numerical simulations in the shearing box approximation (for a detailed description of the shearing box model, see Hawley et al. (1995)). We have assumed, as done in most of the literature on the subject, the simplest case with no vertical stratification and gravity. The box has size  $L \times 4 \times 1$  in the  $x$ ,  $y$  and  $z$  directions, respectively, with  $L$  varying from 1 to 8. Here we will discuss, in particular, the two simulations performed at the highest resolution, one with  $L = 1$  and a grid of  $128 \times 512 \times 128$  points and the second with  $L = 4$  and a grid of  $512 \times 512 \times 128$  points. In all the simulations the sound speed  $c_s$  and the plasma  $\beta = p_{gas}/p_{mag}$  are fixed to values of 4.56 and  $10^4$ , respectively. With these choices the fastest growing MRI mode has a vertical wavelength close to  $1/3$ . The MHD equations are solved in conservative form using

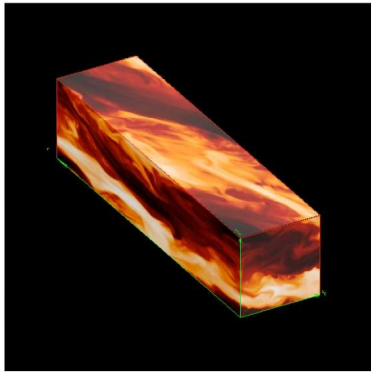


**Fig. 1.** 3D view of the computational box for the  $L = 1$  case, on each face we show the 2D distribution of the longitudinal component of magnetic field in the corresponding plane.

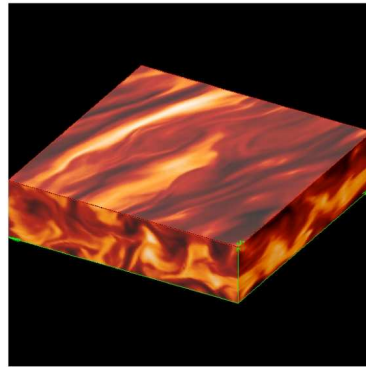


**Fig. 2.** 3D view of the computational box for the  $L = 4$  case, on each face we show the 2D distribution of the longitudinal component of magnetic field in the corresponding plane.

the isothermal MHD module available in the PLUTO code (Mignone et al. 2007; Mignone 2007).

Figures 1 and 2 display the two computational boxes considered, with distributions of the longitudinal component of magnetic field at maxima of angular momentum transport. The box with  $L = 1$  shows an ordered structure corresponding to the channel solution, which is instead absent in the  $L = 4$  case.

In Fig. 3 we show the volume averaged Maxwell stresses  $\langle w_{xy} \rangle = -\langle B_x B_y \rangle$  as a function of time for the two cases considered. We concentrate on the Maxwell stresses because they give the largest contribution to the total stresses exceeding the Reynolds stresses on average by a factor of about 5. We have normalized the stresses to the pressure, thus the values shown in the figure correspond to the  $\alpha$  parameter (Shakura & Sunyaev 1973). The upper panel, corresponding to  $L = 1$ , shows the characteristic intermittent behavior described above. A striking difference appears if we compare this case with the one having an aspect ratio of 4, in which the spikes are absent. Because of the presence of the peaks, the time-averaged value of  $\alpha$  for  $L = 1$  exceeds the other

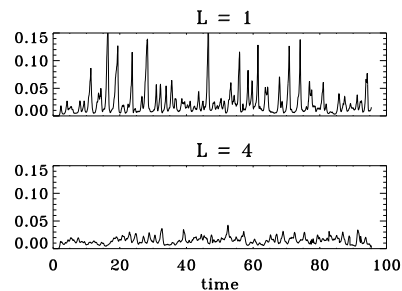


**Fig. 3.** Time histories of the Maxwell stresses averaged over the computational box and normalized to the pressure for the high resolution simulations. The two panels correspond to cases with  $L = 1$ , and 4. Note that time is in units of the rotation time.

case by approximately a factor of 2. The distinctive behavior of the case with  $L = 1$  is due to the presence of channel solutions that are otherwise absent in the simulation with larger aspect ratios. Our results show that the simulations performed with aspect ratios close to unity over-emphasize the role of the channel solutions and may lead to misleading results (Bodo et al. 2008).

### 3. Deceleration of relativistic jets and FRI radiosources

Historically, the extragalactic radio sources have been classified into two categories (Fanaroff & Riley 1974) based upon their radio morphology: a first class of object with jet-dominated emission and showing two-sided jets was named FR I, a second one, with lobe-dominated emission was called FR II (or “classical doubles”). Besides morphology, FR I and FR II radio sources were discriminated in power as well: objects below  $\sim 2 \times 10^{25} h_{100}^2 \text{ W Hz}^{-1} \text{ str}^{-1}$  were typically referred as FR I sources. A more illuminating criterion has been found by Owen & Ledlow (1994) who plotted the radio luminosity against the optical absolute magnitude of the host galaxy: they found the bordering line of FR I to FR II regions correlating as  $L_R \propto L_{opt}^{1.7}$ , i.e. in a luminous galaxy more radio power is required to form a FR II radio sources. This correlation is important since can be interpreted as an indication that the environment may play a crucial role in determining the source structure. The above argument yields the basic question of the origin of FR I/FR II dichotomy, whether intrinsic or ambient driven.

The extrinsic explanations assume that, apart from the total power, FR I and FR II jets are basically similar close to the nucleus and that differences in the environment are able to destabilize, possibly via onset of turbulence in the flow, and decelerate FR I jets effectively, while FR II jets succeed to propagate, nearly unchanged, up to the working surface to produce the hot-spots (Bicknell 1995; Komissarov 1990; Bowman et al. 1996). A possible clue for discriminating among these two kind of interpretations (Gopal-Krishna & Wiita 2000) was the observations of six HYbrid MORphology Radio Sources (HYMORS) that show FR I morphology on one side of the core and FR II morphology on the other one: this is a clear indication that the environment play a basic role in determining the radio source appearance. Moreover statistical analysis of a sample of radio sources, observed with the VLBI at milliarcsecond scales, yielded Giovannini et al. (2001) to conclude that FR I and FR II, de-

spite showing different kpc-scale morphologies, have all the Lorentz factors in the range 3-10 on the parsec scale.

According to the above reasoning, AGN jets are therefore relativistic, and thus supersonic, on parsec scale irrespective of their morphological classification. On the kpc-scale FR II jets may still be relativistic in most cases due to the observed one-sidedness, commonly interpreted as Doppler boosting, while two-sidedness observed in FR I jets is strongly indicative of non relativistic bulk velocities. A key point in the understanding the physics of radio jets is therefore to explain way and how collimated outflows, that are likely to be undifferentiated on the parsec scale, separate in two distinct classes at the kpc-scale.

In order to study this problem we have performed high-resolution hydrodynamic simulations (see Table 1, last column) in which we follow the evolution of a perturbed relativistic jet as it propagates in a homogeneous stationary ambient medium. Perturbations grow as a consequence of the velocity shear instabilities and lead to entrainment of external medium and to jet deceleration. The main questions we address are the dependence of the entrainment and deceleration processes on the jet physical parameters and the kind of structure that the jet acquires as the result of these processes. The simulations have been carried out with the relativistic module of the PLUTO code (Mignone et al. 2007). In table 1 we summarize the parameters of all the cases that we considered.

As we shall discuss below, the main parameter governing the jet behavior and the entrainment properties results to be the density ratio  $\eta$ , while the Mach number plays only a minor role. Our discussion will concentrate on cases A, B and E: cases A and B are representatives of low and high  $\eta$  values, case E show instead what can be the effects of a higher Mach number.

A quantitative estimate of the jet deceleration can be obtained by plotting the Lorentz factor as a function of the longitudinal coordinate  $y$ . Figure 4 shows the maximum value of

**Table 1.** Parameter set used in the numerical simulation model, the second column refers to Lorentz factor  $\gamma_b$ , the third to the Mach number, the fourth to the relativistic Mach number, the fifth to the ratio of proper densities, the sixth to number of mesh points on jet radius, the seventh the physical domain in units of jet radii and the last one the numerical domain

Case	$\gamma_b$	M	$M_r$	$\eta$	pts/beam	$L_x \times L_y \times L_z$	$N_x \times N_y \times N_z$
A	10	3	28.3	$10^2$	20	$50 \times 150 \times 50$	$324 \times 1200 \times 324$
B	10	3	28.3	$10^4$	20	$60 \times 75 \times 60$	$344 \times 600 \times 344$
C	10	3	28.3	$10^4$	12	$50 \times 75 \times 50$	$172 \times 300 \times 172$
D	10	30	300	$10^4$	20	$50 \times 150 \times 50$	$324 \times 1050 \times 324$
E	10	30	300	$10^2$	12	$24 \times 200 \times 24$	$144 \times 560 \times 144$

$\gamma$  at constant  $y$ -planes together with its volume average, defined as

$$\gamma_{\text{av}} = \frac{\int \gamma g(\gamma) dx dz}{\int g(\gamma) dx dz}, \quad (1)$$

where  $g(\gamma)$  is a filter function to select the relativistic flows:

$$g(\gamma) = \begin{cases} 1 & \text{for } \gamma \geq 2, \\ 0 & \text{for } \gamma < 2. \end{cases} \quad (2)$$

For case B one can see that the deceleration occurs both in  $\gamma_{\text{max}}$  (the flow velocity, although still relativistic, shows a strong decrease from its initial value) and in  $\gamma_{\text{av}}$ , which indicates a global effect, whereas in cases A and E the central part of the jet continues to be almost unperturbed and only thin external layers are decelerated.

We now look at the structure that the jet has acquired as a result of the entrainment effects. We consider case B ( $M = 3$ ,  $\eta = 10^4$ ) that shows the most pronounced effect of the interaction with the ambient medium. In Fig. 5 we plot the jet mass distribution as a function of  $\gamma\beta$  at the position  $y = 37.5$  at  $t = 400$  (dashed line) and at  $t = 600$  (solid line). The figure shows the formation of two sharp peaks, one at high  $\gamma\beta$  and the other at velocities  $\gamma\beta \sim 0.2$ , with considerably less material at intermediate velocities. This implies that the jet structure has two well defined velocity components with a steep shear layer between them.

Recently several authors, e.g. (Chiaberge et al. 2000; Piner & Edwards 2004; ?), in order to explain observational properties of FR-I radio sources and their

beamed counterparts (BL Lac objects), have proposed that they are produced by jets characterized by a velocity structure in which an inner core maintains a highly relativistic velocity and is surrounded by material that has been slowed down by the interaction with the ambient medium. A structure of this type has been called “spine-layer”. The appearance of a jet with a spine-layer configuration is different when viewed at different angles.

In our calculations, a “spine-layer” velocity structure has been obtained self-consistently as the result of a well defined physical process, i.e. the interaction of the outer jet layers with the ambient material, driven by jet instabilities. In particular we have found that, in the strongly underdense case  $\eta = 10^4$ , the jet acquires a velocity structure in which the inner core maintains a highly relativistic velocity and is surrounded by material that has been slowed down by the interaction with the ambient medium. Therefore we attempt a comparison of radio maps constructed from the simulated jets with observations of FR-I jets. To this purpose, we compute synthetic maps by integrating the synchrotron emissivity along the line of sight. For the sake of simplicity we assume the emissivity to be proportional to the proper density of the jet material multiplied by the appropriate boosting or deboosting factor, i.e. by the quantity

$$\epsilon(x, y, z) = \left[ \frac{1}{\gamma(1 - \beta \cos \theta)} \right]^{2+\alpha}, \quad (3)$$

where  $\alpha$  is the spectral index of the radio flux (we take  $\alpha = 0.5$ ).

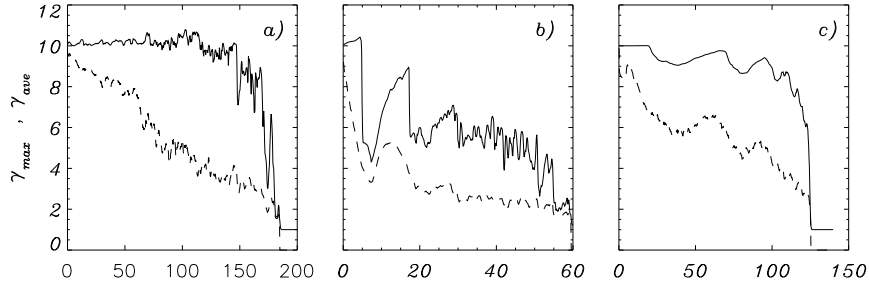


**Fig. 4.** Plots of the maximum value (solid line) and of an average value (dashed line) of  $\gamma$  as functions of the longitudinal coordinate  $y$  along the jet. The left panel refer to case A, the center panel to case B and the right panel to case E.

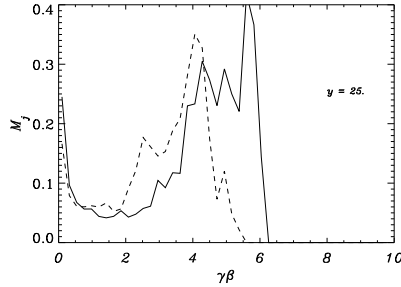


**Fig. 5.** Jet mass distribution as a function of  $\gamma\beta$  at the locations  $y = 12.5, 25, 37.5$  at  $t = 400$  (dashed line) and  $t = 600$  (solid line)

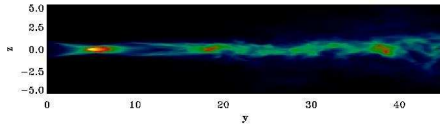


**Fig. 6.** Synthetic map for the jet of case B with an inclination of  $20^\circ$  with respect to the line of sight.

The synthetic maps are plotted in Figs. 6 and 7 for inclination angles of the jet axis to the line of sight of  $20^\circ$  and  $60^\circ$  respectively. In the small angle case, the relativistic jet  $\gamma \sim 4 \div 5$  core emission dominates. Emission is present

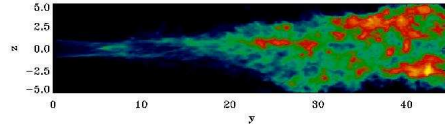


**Fig. 7.** Synthetic map for the jet of case B with an inclination of  $60^\circ$  with respect to the line of sight.

along the whole jet and some knots can be recognized, the most brilliant being the first one; knots correspond to the oblique shocks in the pressure maps. Increasing the inclination angle, the dominant contribution to emission is due to relatively slow material, whose fraction in the first part of the jet is very low, so that emission is almost absent, apart from the first knot that is still visible at lower brightness. The fraction of slow material starts to increase at a distance of about 15 radii where the jet appears to have a sudden increase in opening angle, due to the formation of a thick layer of slowly moving material which dominates the emission at larger distances. We can also observe some limb brightening, explained by the emission coming from the slow layer surrounding the deboosted relativistic core. A similar limb brightening effect is shown, for example, in the radio source B2 1144+35, whose VLBI map is shown in Fig. 8

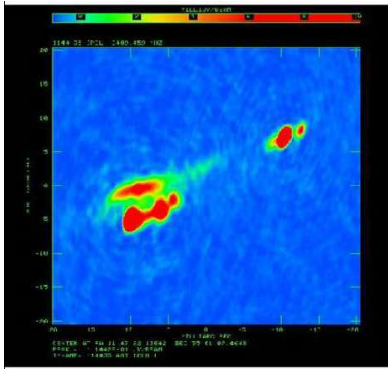


**Fig. 8.** VLBI image at 8.4 GHz of B2 1144+35 (Giovannini et al. 2007).

#### 4. Conclusions

We have presented the results of high resolution numerical simulations concerning the problem of angular momentum transport in accretion disks and the deceleration of relativistic jets. Our simulations of the magnetorotational instability in accretion disks have shown that the results obtained in the shearing box approximation require caution in their applicability to the whole disk. Global simulations with sufficient resolution are at the edge of the present capabilities. An intermediate step could be that of introducing the effects of gravity and density stratification in the shearing box approximation keeping a sufficiently high resolution, since, at the present, simulations of this kind are still at relatively low resolution (Fleming & Stone 2003).

The results on relativistic jets show that the main parameter that determines the efficiency of the entrainment of external material is the density ratio between the jet and the ambient medium. Low density jets are more affected by the entrainment and acquire a structure in which a relativistic core is surrounded by a slower layer. We have also examined the qualitative observational consequences of this structure. The next step would be that of including magnetic effects.

*Acknowledgements.* The numerical calculations have been performed at CINECA in Bologna, Italy,

thanks to INAF. This work has been supported by MIUR by PRIN 2005.

#### References

- Balbus, S. A. 2003, *Ann. Rev. Astron. Astrophys.*, 41, 555
- Balbus, S. A., & Hawley, J. F. 1991, *ApJ*, 376, 214
- Bicknell, G. V. 1995, *ApJS*, 101, 29
- Bodo, G., et al. 2008, *A&A*, in press.
- Bowman, M., Leahy, J. P., & Komissarov, S. S. 1996, *MNRAS*, 279, 899
- Chiaberge, M., Celotti, A., Capetti, A., & Ghisellini, G. 2000, *A&A*, 358, 104
- Fanaroff, B. L. & Riley, J. M. 1974, *MNRAS*, 167, 31P
- Fleming, T., & Stone, J. M. 2003, *ApJ*, 585, 908
- Giovannini, G., et al. 2001, *ApJ*, 552, 508
- Giovannini, G., Giroletti, M., & B., T. G. 2007, astro-ph arXiv:0708.3902v1
- , et al. 2004, *ApJ*, 600, 127
- Gopal-Krishna, & Wiita, P. J. 2000, *A&A*, 363, 507
- Hawley, J. F., & Balbus, S. A. 1992, *ApJ*, 400, 595
- Hawley, J. F., Gammie, C. F., & Balbus, S. A. 1995, *ApJ*, 440, 742
- Hawley, J. F. 2001, *ApJ*, 554, 534
- Hawley, J. F., Balbus, S. A. & Stone, J. M. 2001, *ApJ*, 554, 49
- Komissarov, S. S. 1990, *Ap&SS*, 171, 105
- Mignone, A., et al. 2007, *ApJS*, 170, 228
- Mignone, A. 2007, *J. Comp. Phys.*, 225, 1427
- Owen, F. N., & Ledlow, M. J. 1994, *The Physics of Active Galaxies*, 54, 319
- Piner, B. G. & Edwards, P. G. 2004, *ApJ*, 600, 115
- Shakura, N. I., & Sunyaev, R. A. 1973, *A&A*, 24, 337
- Sano, T. & Inutsuka, S. 2001, *ApJ*, 561, L179
- Sano, T., Inutsuka, S., Turner, N. J. & Stone, J. M. 2004, *ApJ*, 605, 321
- Sano, T. & Stone, J. M. 2002, *ApJ*, 570, 314
- Turner, N. J., Stone, J. M., Krolik, J. H. & Sano, T. 2003, *ApJ*, 593, 992